THE JOURNAL OF BIOLOGICAL CHEMISTRY Vol. 274, No. 37, Issue of September 10, pp. 26439–26447, 1999
Printed in U.S.A.

Clinical Severity and Thermodynamic Effects of Iron-responsive Element Mutations in Hereditary Hyperferritinemia-Cataract Syndrome*

(Received for publication, May 25, 1999)

Charles R. Allerson‡, Mario Cazzola§, and Tracey A. Rouault‡¶

From the ‡Cell Biology and Metabolism Branch, NICHD, National Institutes of Health, Bethesda, Maryland 20892 and §Department of Internal Medicine and Medical Therapy, Internal Medicine and Medical Oncology, University of Pavia Medical School and IRCCS Policlinico S. Matteo, 27100 Pavia, Italy

Hereditary hyperferritinemia-cataract syndrome (HHCS) is a novel genetic disorder characterized by elevated serum ferritin and early onset cataract formation. The excessive ferritin production in HHCS patients arises from aberrant regulation of L-ferritin translation caused by mutations within the iron-responsive element (IRE) of the L-ferritin transcript. IREs serve as binding sites for iron regulatory proteins (IRPs), iron-sensing proteins that regulate ferritin translation. Previous observations suggested that each unique HHCS mutation conferred a characteristic degree of hyperferritinemia and cataract severity in affected individuals. Here we have measured the *in vitro* affinity of the IRPs for the mutant IREs and correlated decreases in binding affinity with clinical severity. Thermodynamic analysis of these IREs has also revealed that although some HHCS mutations lead to changes in the stability and secondary structure of the IRE, others appear to disrupt IRP-IRE recognition with minimal effect on IRE stability. HHCS is a noteworthy example of a human genetic disorder that arises from mutations within a protein-binding site of an mRNA cis-acting element. Analysis of the effects of these mutations on the energetics of the RNA-protein interaction explains the phenotypic variabilities of the disease state.

Several reports have described a new autosomal dominant disorder called hereditary hyperferritinemia-cataract syndrome (HHCS)[1] (1–12). This condition is characterized by a combination of elevated levels of serum ferritin and congenital nuclear cataract. Human ferritin is composed of two different types of subunit (H-ferritin and L-ferritin), although the relative proportion of each subunit in the ferritin copolymer varies among tissues (13). Through the use of monoclonal antibodies specific for either H- or L-ferritin, the excess serum ferritin in HHCS patients has been shown to be predominantly L-ferritin (3, 7). A close relationship has also been established between monocyte L-ferritin content and serum ferritin concentration (7), suggesting that the excess production of L-ferritin in cells is directly responsible for the hyperferritinemia. Although serum ferritin is thought to reflect body iron stores, individuals with HHCS do not appear to suffer from iron overload (1, 2).

The expression of both H-ferritin and L-ferritin is normally regulated according to intracellular iron concentration by means of iron-responsive elements (IREs) that are found within the 5′-untranslated regions of their transcripts (14, 15). These regulatory elements interact with the iron regulatory proteins IRP1 and IRP2, which are both capable of sensing cellular iron status. Under conditions of intracellular iron depletion, both IRP1 and IRP2 bind to IREs with high affinity. The binding of an IRP to the ferritin IRE prevents the binding of the 43 S translation initiation complex to the transcript (16, 17) and thus blocks translation of the ferritin protein. When intracellular iron concentrations rise, IRP1 acquires a [4Fe-4S] cluster that prevents its association with IREs and activates its function as a cytosolic aconitase (reviewed in Refs. 18 and 19). Under the same conditions, IRP2 is targeted for degradation by the proteasome (20, 21). In the absence of bound IRP, the ferritin transcript is readily translated. IREs are also found within the transcripts of other iron uptake and iron utilization proteins and have a highly conserved stem-loop secondary structure (Fig. 1*b*).

The absence of iron overload in HHCS patients suggested that the elevated serum ferritin resulted from misregulation of L-ferritin expression. Analysis of the L-ferritin genetic locus in HHCS patients led to the identification of mutations occurring within the IRE of L-ferritin (Fig. 1*a*), most of them occurring as single point mutations (2, 4, 7, 9, 11), although a double point mutation (7) and a 29-base deletion (8) have also been reported. Several of these mutations have been shown to disrupt IRE-IRP binding *in vitro*, and it seems likely that the others would have similar effects, leading to increased expression of L-ferritin *in vivo*. As patients with HHCS have been characterized, however, it has become clear that not all are equally affected by the disorder. Some patients have serum ferritin levels more than 5-fold higher than normal and a history of severe cataracts, whereas others have only slightly elevated serum ferritin and are asymptomatic for cataract.

Studies of non-HHCS IRE mutations have demonstrated that some mutations affect *in vitro* IRE-IRP binding affinities much more severely than others (22), so we hypothesized that all or part of the range of severity seen among HHCS patients might arise from differences in the ability of each mutation to disrupt IRE-IRP interactions. We were also interested in evaluating whether HHCS mutations might affect the affinities of IRP1 and IRP2 differently. As studies have demonstrated, both IRP1 and IRP2 are capable of recognizing their own unique substrates *in vitro* (23, 24). In an effort to identify any corre-

* This work was supported in part by grants from MURST, Rome, and IRCCS Policlinico S. Matteo, Pavia (to M. C.). The costs of publication of this article were defrayed in part by the payment of page charges. This article must therefore be hereby marked "*advertisement*" in accordance with 18 U.S.C. Section 1734 solely to indicate this fact.

¶ To whom correspondence should be addressed: Bldg. 18T, Rm. 101, NICHD, 9000 Rockville Pike, National Institutes of Health, Bethesda, MD 20892. Tel.: 301-496-6368; Fax: 301-402-0078; E-mail: trou@helix.nih.gov.

[1] The abbreviations used are: HHCS, hereditary hyperferritinemia-cataract syndrome; IRE, iron-responsive element; IRP, iron regulatory protein; ER, endoplasmic reticulum.

lation between HHCS severity and IRP affinity, and to reveal any differences in the behavior of the two IRPs, we determined the dissociation constants (K_D values) for the binding of the HHCS IREs to both IRP1 and IRP2.

The identification of the HHCS mutations has also provided us with an opportunity to understand more precisely the structural features of the IRE required for IRP binding. Recent NMR studies of the consensus IRE have revealed intriguing features of its three-dimensional structure (25–27); however, it has been difficult to ascertain the importance of those features for IRP recognition. We have used thermal denaturation methods to determine the effects of each HHCS mutation on the thermodynamic stability of the IRE. Analysis of the resulting melting curves has allowed us to identify HHCS mutations that are likely to disrupt direct contacts between the IRE and IRPs and other mutations located both near and distant from putative contact points whose predominant effect is to alter IRE stability.

EXPERIMENTAL PROCEDURES

Synthesis of Wild-type and Mutant RNAs—The RNAs used for both the band-shift competition assays and thermal denaturation experiments were prepared by T7 RNA polymerase transcription from single-stranded DNA templates using published methods (28). A series of 94-nucleotide template DNAs were used to encode the 77-nucleotide RNAs and were purchased from either Operon Technologies, Inc. (Alameda, CA) or Integrated DNA Technologies (Coralville, IA). For example, the template for the wild-type L-ferritin IRE was 5′-CTGGAAGAGA GTCCCCGGAT CTGTTCCGTC CAAACACTGT TGAAGCAAGA GACAGACCCG CGGGACCGCC GAACTCC*TAT AGTGAGTCGT ATTA*-3′ (the T7 RNA polymerase promoter region is italicized). A typical 1-ml transcription reaction contained 40 mM Tris-HCl (pH 7.5), 20 mM $MgCl_2$, 5 mM dithiothreitol, 1 μM spermidine, 0.01% Triton X-100, 2 mM each NTP, 0.2 μM DNA template, and 1.5 units/μl T7 RNA polymerase (Life Technologies, Inc.) and was incubated at 37 °C for 3 h. Transcribed RNAs were purified on 8% (7 M urea) polyacrylamide gels, extracted from the gel, and desalted by dialysis against a solution of 10 mM potassium phosphate (pH 7.5) and 10 mM KCl using Spectra/Por CE 500 molecular weight cut-off DispoDialyzers (Spectrum). All RNAs were quantitated by UV absorbance spectroscopy and were folded prior to use by heating to 95 °C for 5 min, followed by renaturation on ice for 20 min.

Synthesis of Radiolabeled Wild-type Ferritin IRE—Internally ^{33}P-radiolabeled wild-type Ferritin IRE was transcribed from the same DNA template described above. RNA was transcribed in a 25-μl transcription reaction containing 40 mM Tris-HCl (pH 7.5), 25 mM $MgCl_2$, 5 mM dithiothreitol, 1 μM spermidine, 0.01% Triton X-100, 4 mM GTP, 4 mM ATP, 4 mM CTP, 0.8 mM UTP, 1.7 μM (125 μCi) [α-^{33}P]UTP (Amersham Pharmacia Biotech), 0.2 μM DNA template, and 2 units/μl T7 RNA polymerase. RNA was purified as described above except that following isolation from the gel the RNA was ethanol-precipitated and resuspended in diethyl pyrocarbonate-treated H_2O. The RNA was quantitated and folded as described above.

Band-shift Competition Experiments—Human IRP1 and IRP2 proteins for these studies were expressed and purified as previously reported (29). All competition reactions were prepared as follows: 0.8 pmol (40 nM) of ^{33}P-labeled wild-type L-ferritin IRE was mixed with either 0, 0.8, 1.6, 4.0, 8.0, or 80.0 pmol (0, 40, 80, 200, 400, or 4000 nM) of unlabeled competitor in the presence of 5% glycerol, 0.025 units/μl RNase inhibitor (5 Prime → 3 Prime, Inc., Boulder, CO), 0.15 mg/ml yeast tRNA, 2 mM dithiothreitol, 25 mM Tris-HCl (pH 7.5), 40 mM KCl, and 0.6 pmol (30 nM) of IRP1 or IRP2. These reactions were incubated at room temperature for 20 min and then electrophoresed on 10% nondenaturing polyacrylamide gels at 130 V for 4 h. After drying, the gels were exposed to either Kodak BioMax MR film or a Molecular Dynamics PhosphorImaging screen.

Calculation of Dissociation Constants K_D and K_{Rel}—Quantitation of band-shift competition gels was performed using a Molecular Dynamics PhosphorImager and the Molecular Dynamics ImageQuant software package. We calculated K_D values using a method previously reported for competition assays (30). Briefly, quantitation of the gels yielded f_0 (the fraction of radiolabeled RNA shifted in the absence of competitor), f (the amount of radiolabeled RNA shifted in lanes with competitor), and f_1, where $f_1 = f/f_0$. From these values, the following equations were used to determine the apparent K_D (K_{app}): $K_{app} = [C]_{free}(f_1/(1 - f_1))$, where $[C]_{free} = [C]_i - [H]_i(f_0 - f)$ and represents the amount of unbound competitor RNA; $[C]_i$ represents the initial concentration of competitor RNA, and $[H]_i$ represents the initial amount of radiolabeled RNA. Using K_{app}, $[H]_{free}$ (the concentration of unbound radiolabeled IRE) and the K_D(known) for the wild-type IRE (as previously reported, see Ref. 23), the following equation can be used to determine K_D(comp), the K_D of the competitor RNA: $K_D(\text{comp}) = (K_{app}K_D(\text{known}))/(K_D(\text{known}) + [H]_{free})$. The relative K_D, K_{Rel}, equals K_D(comp)/K_D(known). For each HHCS mutant, K_D(comp) is listed as the mean of at least three separate experiments ±1 S.D. in Table I. $\Delta\Delta G_{25}$(complex) was calculated from $RT \ln (K_{Rel})$.

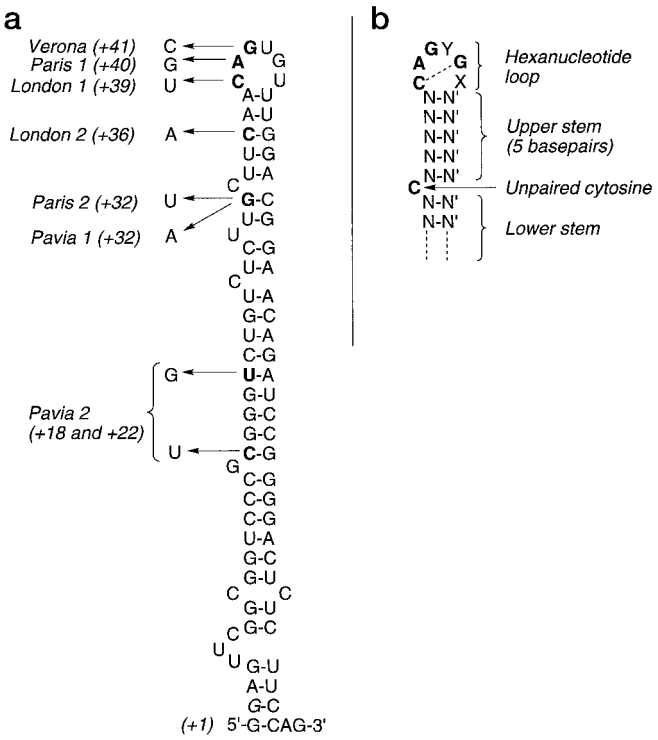

FIG. 1. **Secondary structures of the L-ferritin IRE and the consensus IRE.** *a,* the positions of the HHCS mutations within the L-ferritin IRE are identified in *bold*, with the *arrow* indicating the observed nucleotide substitution. The numbering of the nucleotide positions is with respect to the transcriptional start site. Each mutation has been named using the name of the city in which it was first identified and characterized (Verona, Verona, Italy; Paris 1 and Paris 2, Paris, France; London 1 and London 2, London, UK; Pavia 1 and Pavia 2, Pavia, Italy). The first 77 nucleotides of the L-ferritin transcript were used throughout these studies; the nucleotide in the +2 position is *italicized* to indicate that the naturally occurring C has been replaced with a G to facilitate transcription with T7 RNA polymerase; *b,* the sequence and secondary structure of the consensus IRE. The hexanucleotide loop has the sequence CAG*Y*G*X*, where *Y* = U or A and *X* = U, C, or A; C-1 and G-5 of the loop form a loop-bridging base pair. The upper stem of 5 base pairs is separated from a lower stem of varying length by an unpaired cytosine.

Statistical Analysis of HHCS Severity Correlations with K_{Rel}—Data were stored, analyzed, and reported with the package Exstatix (Select Micro Systems, Inc., Yorktown Heights, NY) and DeltaGraph Pro 3 (DeltaPoint, Inc., Monterey, CA). Results were expressed as a mean ± 1 S.D. unless otherwise stated. Simple and multiple linear regression and nonlinear regression analyses were employed to identify the parameters most closely related to K_{Rel}. The correlations of ln (serum ferritin) *versus* $1/K_{Rel}$ were statistically significant for both IRP1 (n = 37, F = 32.886, $p < 0.00001$) and IRP2 (n = 37, F = 29.435, $p < 0.00001$). The fit of ln (max ferritin) *versus* $1/K_{Rel}$ correlated with R^2 = 0.978 (IRP1) and R^2 = 0.991 (IRP2). Frequencies were compared by nonparametric analysis (2 × 2 table). p values of less than 0.05 were considered statistically significant.

Thermal Denaturation (T_m) Experiments—All thermal denaturation experiments were performed on a Beckman DU 640 UV-visible spectrophotometer equipped with a high performance temperature controller and a 6-position mini-cuvette holder. All measurements were made using 0.350-ml volume Teflon-stoppered quartz cuvettes with a 1.0-cm

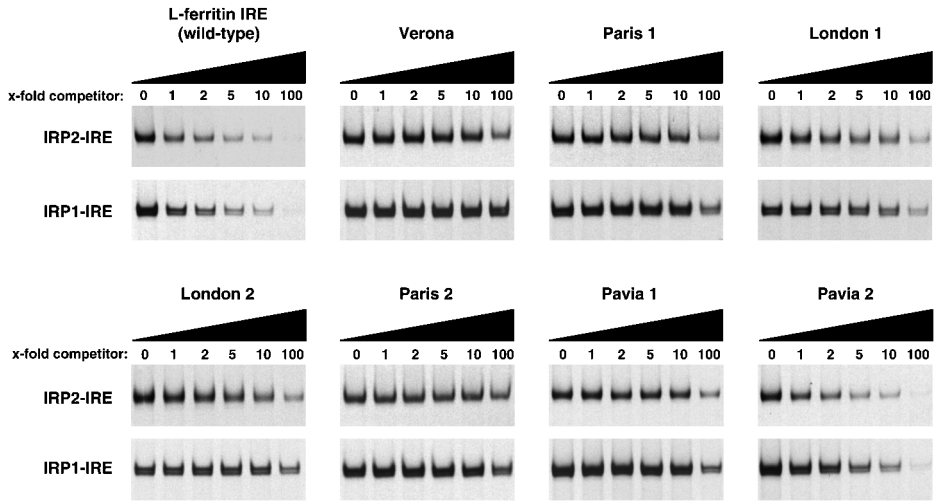

FIG. 2. **Band-shift competition assays of IREs containing HHCS mutations.** Band-shift competition experiments were performed in order to determine the binding affinities (K_D values) of IREs containing HHCS point mutations. Radiolabeled (^{33}P) wild-type L-ferritin IRE (0.8 pmol) was incubated with either human IRP1 or human IRP2 (0.6 pmol) in the absence or presence of increasing quantities (0, 0.8, 1.6, 4.0, 8.0, and 80.0 pmol) of unlabeled competitor IRE that contained either no mutations (wild-type L-ferritin) or a single HHCS mutation. These samples were electrophoresed on 10% nondenaturing polyacrylamide gels, and the amount of ^{33}P-labeled IRE in an IRP-shifted band was measured in each lane. The gels were visualized by autoradiography and by exposure to a phosphorimaging screen, which permitted the quantitation of the amount of RNA shifted in each lane. Sections of each gel containing the IRP-shifted RNA are assembled above. From these images we can identify mutations that severely reduce IRE affinity (Verona, Paris 2, and Paris 1), moderately reduce affinity (London 1, London 2, and Pavia 1), and minimally alter affinity (Pavia 2).

TABLE I

Changes in dissociation constants and thermodynamic stabilities of IRP1 and IRP2 complexes with IREs containing HHCS mutations

Dissociation constants (K_D) were determined from band-shift competition experiments in which human IRP1 or human IRP2 were incubated with ^{33}P-labeled L-ferritin IRE in the absence or presence of increasing quantities of an unlabeled IRE containing the indicated HHCS mutation (see "Experimental Procedures" and Fig. 2). The average of at least three separate experiments ± 1 S.D. is listed. The relative dissociation constant, K_{Rel}, was calculated from the ratio of the K_D of the mutated IRE over the K_D of the wild-type L-ferritin IRE. The change in free energy of the resultant IRE·IRP complexes was calculated from $\Delta\Delta G_{25}(\text{complex}) = RT \ln K_{Rel}$.

HHCS mutation	IRP1 binding			IRP2 binding		
	K_D	K_{Rel}	$\Delta\Delta G_{25}$(complex)	K_D	K_{Rel}	$\Delta\Delta G_{25}$(complex)
	pM		*kcal/mol*	*pM*		*kcal/mol*
L-Ferritin IRE	50 ± 2	1.0	0.0	41 ± 2	1.0	0.0
Verona	109,000 ± 7000	2200.0	4.6	9,100 ± 600	220.0	3.2
Paris 1	11,000 ± 1000	220.0	3.2	3,400 ± 200	83.0	2.6
London 1	460 ± 70	9.2	1.3	230 ± 70	5.6	1.0
London 2	1,800 ± 400	36.0	2.1	400 ± 90	9.8	1.4
Paris 2	31,000 ± 4000	620.0	3.8	9,100 ± 800	220.0	3.2
Pavia 1	3,700 ± 500	74.0	2.5	2,600 ± 300	63.0	2.5
Pavia 2	75 ± 5	1.5	0.2	71 ± 2	1.7	0.3
Truncated	68 ± 3	1.4	0.2	66 ± 4	1.6	0.3

light path. To ensure that RNAs were monomers, melting curves for each RNA were measured at a range of RNA concentrations (0.1 to 10 μM). All RNAs appeared to behave as monomers and gave similar melting profiles on both heating and cooling (data not shown). Data for thermodynamic curve-fitting analysis were collected on 1.0 μM RNA samples in 20 mM potassium phosphate (pH 7.5) and 40 mM KCl. Both A_{260} and A_{280} were measured at 0.5 °C intervals as the temperature was ramped from 18 to 95 °C at a rate of 0.5 °C/min.

Curve-fitting Analysis of Thermal Denaturation Data—Data were analyzed using the MeltFit software package designed and provided by David Draper (31). From the raw absorbance data, the first derivative of the absorbance *versus* temperature plot was determined using the Savitsky-Golay option in MeltFit and was normalized to the absorbance at 25 °C. In each case except for the Pavia 2 mutant, fitting of the first derivative curves to four sequential transitions was performed simultaneously at both 260 and 280 to improve the quality of the fit. From the ΔH and T_m values of each transition provided by MeltFit, values for both ΔG_{25} and ΔS_{25} were calculated as $\Delta G_{25} = \Delta H\,(1 - T/T_m)$ and $\Delta S_{25} = (\Delta H - \Delta G_{25})/T$, where T = 298.15 K, and T_m is the melting temperature, also expressed in Kelvin. Theoretical values of ΔG, ΔH, and ΔS (at 1 M NaCl) were determined for the wild-type L-ferritin IRE using the Turner Rules for nearest neighbor approximation (32).

RESULTS

We used band-shift competition assays to determine the affinities of IRP1 and IRP2 for IREs containing HHCS mutations. These experiments measured the ability of the mutant IREs to compete with ^{33}P-labeled wild-type L-ferritin IRE for the binding of the IRPs, as detected by the gradual disappearance of a shifted band on the gel in the presence of increasing amounts of unlabeled competitor. As a control, we included an experiment in which wild-type L-ferritin IRE was used as the competitor. In these and all subsequent experiments, we used RNA oligonucleotides that had been designed to include the first 77 nucleotides of the L-ferritin transcript in an effort to conserve some of the natural context of the IRE (Fig. 1*a*). These constructs differed from the actual transcript only in lacking the normal 5′ cap modifications and having a G instead of C at the +2 position to permit efficient translation by T7 RNA polymerase. Gel sections showing the IRP-shifted band from each experiment have been assembled in Fig. 2. The appearance of the IRP1-shifted band as a fine doublet is the result of

changes in the oxidative state of a disulfide couple that does not affect IRE binding activity (data not shown).

By visual inspection, we can readily distinguish the mutations that most severely impair the ability of the IRE to compete for IRP binding from those that only modestly impair competition. The most ineffective competitors are the Verona, Paris 2, and perhaps Paris 1 mutations. IREs containing these mutations only begin to show significant competition when present at 100-fold excess. Another group of mutations, including London 1, London 2, and Pavia 1, compete effectively at somewhat lower concentrations, between 5- and 10-fold excess. In contrast, the Pavia 2 mutation nearly rivals the wild-type L-ferritin IRE in its ability to compete for binding. Qualitatively, the competition profile for each mutation appears to be similar for both IRPs.

To characterize further these mutations, we quantitated the amounts of shifted and unshifted RNA in each of the competition experiments. By using the previously determined K_D values for the interactions of a consensus IRE with IRP1 (50 pM) or IRP2 (30 pM) (23), we were able to calculate the K_D values of each mutant IRE, and the ratio of the K_D(mutant) to K_D(wild type), expressed as K_{Rel} (Table I). By this method, $K_{Rel} > 1$ indicates weaker binding, whereas $K_{Rel} < 1$ indicates stronger binding. The K_D values calculated in control competition experiments with wild-type L-ferritin were 50 ± 2 pM for IRP1, and 41 ± 2 pM for IRP2, in good agreement with the previously reported values. The Verona mutation had the lowest affinity for both IRP1 and IRP2, with K_D values of about 109 (2200-fold reduction) and 9.1 nM (220-fold reduction), respectively. The Paris 2 mutation also showed large reductions in affinity, 620-fold for IRP1 and 220-fold for IRP2. Although the Pavia 1 and Paris 2 mutations involve the same nucleotide position, immediately 5′ of the conserved unpaired cytosine, the Pavia 1 mutation is less deleterious to binding. The Paris 1 mutation caused a 220-fold reduction in affinity for IRP1 but had a somewhat more modest effect on IRP2, with only an 83-fold change in K_D. Both of the London 1 and London 2 mutations retained modest affinities for the IRPs. The K_D values of the IRPs for the Pavia 2 mutant differed from the wild-type affinities by less than 2-fold, similar to the those measured for a wild-type L-ferritin IRE truncated immediately below the C23:G57 base pair (see Fig. 1*b*; K_D and K_{Rel} for the truncated IRE are listed in Table I, but the corresponding gel slices are not shown in Fig. 2). One striking pattern that emerged from the measurement of the K_D values is that each mutation appears to diminish affinity for IRP1 affinity more than for IRP2. However, the arrangement of the mutations from highest to lowest affinity remains the same for either protein.

Data regarding the serum ferritin in HHCS patients was compiled from several sources (1–12). For both IRP1 and IRP2, we plotted the K_{Rel} of each mutation *versus* its clinically measured values of serum ferritin (Fig. 3), and in both cases there appeared to be a correlation. Nonlinear regression analysis (regression of ln (serum ferritin) *versus* $1/K_{Rel}$) showed that there was a significant relationship between serum ferritin and K_{Rel} values of both IRP1 and IRP2. As Fig. 3 illustrates, serum ferritin levels vary dramatically among patients with the same mutation or even within a single patient on different occasions. Yet we noticed that the greatest serum ferritin for each mutation, denoted as max ferritin and appearing in Fig. 3 as *filled circles*, appears to be strongly linked to K_{Rel}. Therefore, we performed regression analysis of ln (max ferritin) *versus* $1/K_{Rel}$ and found further evidence of a correlation for both IRP1 and IRP2.

The absence of a quantitative measurement for the severity of cataract in HHCS patients made it difficult to establish any

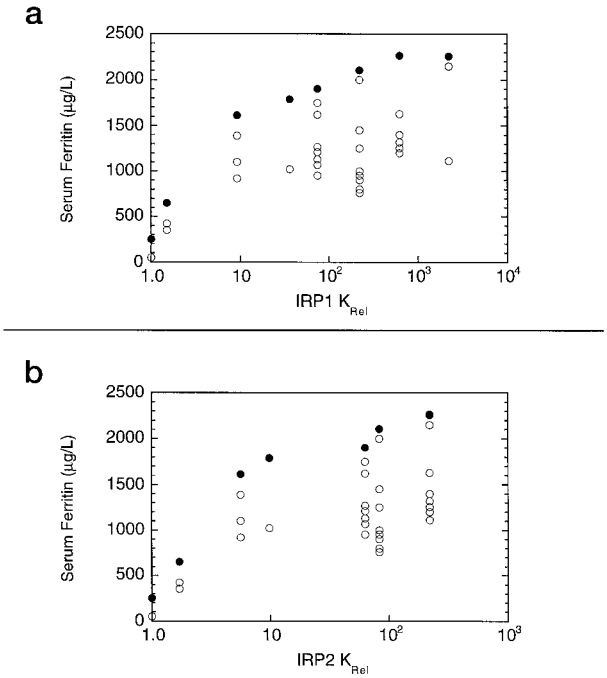

FIG. 3. **Correlation of serum ferritin with K_{Rel}(IRP1) and K_{Rel}(IRP2) for HHCS mutations.** *a,* plot of the serum ferritin observed for a given HHCS mutation *versus* the K_{Rel} of an IRE with that mutation for IRP1 ($K_{Rel} = K_D$(mutant)/K_D(wt)). Maximal values of serum ferritin (max ferritin) are shown as *filled circles*. Nonlinear regression of ln (serum ferritin) *versus* $1/K_{Rel}$(IRP1) yielded ln (serum ferritin) = 7.210 − 1.619($1/K_{Rel}$), (n = 37, F = 32.886, $p < 0.00001$), whereas regression of ln (max ferritin) *versus* ($1/K_{Rel}$) yielded ln (max ferritin) = 7.640 − 1.995 ($1/K_{Rel}$), R^2 = 0.978. *b,* plot of the serum ferritin *versus* K_{Rel} for IRP2. Again, maximal values of serum ferritin (max ferritin) are shown as *filled circles*. Nonlinear regression of ln (serum ferritin) *versus* $1/K_{Rel}$(IRP2) yielded ln (serum K_{Rel} ferritin) = 7.236 − 1.762($1/K_{Rel}$), (n = 37, F = 29.435, $p < 0.00001$), whereas regression of ln (max ferritin) *versus* ($1/K_{Rel}$) yielded ln (max ferritin) = 7.6908 − 2.1204 ($1/K_{Rel}$), R^2 = 0.991.

clear relationship between variations in K_{Rel} and severity of cataract. We therefore defined cataract as severe when there was a marked loss in visual acuity in the 1st decades (with some individuals requiring surgery), mild when the defect in visual acuity could be corrected with the use of appropriate eyeglasses, and asymptomatic when it did not impair visual acuity. By using nonparametric analysis, values of K_{Rel}(IRP1) <100 and K_{Rel}(IRP2) <80 were significantly associated with asymptomatic to mild cataract, whereas K_{Rel}(IRP1) >100 or K_{Rel}(IRP2) >80 were found in association with mild to severe cataract (χ^2 = 29.68, $p < 0.00001$). The characteristics of each mutation are summarized in Table II.

Because the consensus IRE has both conserved primary sequence elements and conserved secondary structure elements, we realized that reductions in affinity in HHCS could be caused by the elimination of a sequence-specific contact (hydrogen bonding, van der Waals contacts, electrostatic interactions), the perturbation of the secondary structure or stability of the IRE (structure-specific effects), or a combination of both. The destabilization of the complex with respect to the wild-type association can be expressed in terms of $\Delta\Delta G_{25}$(complex) and is readily calculated from RT ln K_{Rel} such that decreases in affinity appear as positive values. The change in free energy of the complexes ranged from 0.2 to 4.6 kcal/mol for IRP1 and 0.3 to 3.2 kcal/mol for IRP2 (Table I). The change in IRE·IRP complex stability should be reflected by the sum of changes in specific intermolecular interactions and changes in the stability of the IRE, which can be expressed as $\Delta\Delta G_{25}$(IRE). In an

TABLE II
Relationships between mutations in the L-ferritin IRE and clinical features of HHCS patients

Molecular lesion in IRE	Range of serum ferritin[a]	Cataract[b]	Comments
Verona (G41C)	1,112–2,259 μg/liter (in 3 affected individuals belonging to a single kindred)	Cataract requiring surgery in the middle age in one individual	Data source, Refs. 1 and 4 Mild to severe cataract
Paris 1 (A40G)	760–2,105 μg/liter (in 13 affected individuals belonging to three kindreds)	Severe visual symptoms appearing in the 1st decade	Data source, Refs. 2, 3, 5, 9, 12 Mild to severe cataract
London 1 (C39U)	918–1,615 μg/liter (in 4 affected individuals belonging to two kindreds)	Visual symptoms appearing in the mid-30s	Data source, Ref. 12 Mild cataract
London 2 (C36A)	1,022–1,788 μg/liter (in several individuals in a single kindred, two of them included in data analysis)	Cataract developing early in life; required surgical correction in a child	Data source, Ref. 11 Mild to severe cataract
Paris 2 (G32U)	1,200–2,264 μg/liter (in 6 affected individuals of variable age belonging to two kindreds)	Visual symptoms appearing late in childhood in one family, around the age of 40 in the other	Data source, Ref. 10 Mild cataract with a marked phenotypic variability
Pavia 1 (G32A)	950–1,900 μg/liter (in 8 affected individuals belonging to two kindreds)	Visual symptoms appearing in childhood	Data source, Refs. 7 and 12 Mild to severe cataract
Pavia 2 (U22G, C18U)	350–650 μg/liter (in 3 affected individuals of variable age belonging to a single kindred)	No visual symptoms but multiple opacities are visible in the lens core by slit-lamp examination	Data source, Ref. 7 Asymptomatic cataract

[a] Normal serum ferritin is 50–250 μg/liter.
[b] Cataract was judged severe when there was a marked loss in visual acuity in the 1st decades (with some individuals requiring surgery), mild when the defect in visual acuity could be corrected with the use of appropriate eyeglasses, and asymptomatic when it did not impair visual acuity.

effort to understand some of these contributions, we used UV thermal denaturation experiments and the fitting of sequential transitions to the resulting melting curves to determine $\Delta\Delta G_{25}$(IRE) (31).

The absorbance of each IRE was monitored at both 260 and 280 nm as the temperature was increased from 18 to 95 °C. From the change in absorbance as a function of temperature, we calculated the first derivative with respect to temperature ($\delta A/\delta T$), and we plotted this *versus* temperature to yield the melting curves shown in Fig. 4. The predicted total ΔG, ΔH, and ΔS for the L-ferritin IRE using the Turner Rules (32) and the secondary structure depicted in Fig. 1 are as follows: $\Delta H = -288.2$ kcal/mol, $\Delta S = -819$ e.u., and $\Delta G = -27.8$ kcal/mol. Because the helical portion of the L-ferritin IRE used here is periodically interrupted by unpaired nucleotides, we expected these IREs to denature as a series of discrete domains and that these would appear as overlapping sequential transitions in the melting profiles. Although we were uncertain about the number of transitions to expect in the unfolding of our IREs, fitting of the melting curve of the wild-type L-ferritin IRE to four sequential transitions yielded total ΔH and ΔG values that were in closest agreement to the predicted values ($\Delta H = 274$ kcal/mol and $\Delta G_{25} = 29.6$ kcal/mol). From our denaturation experiments, ΔH, ΔG, and ΔS are reported as positive values.

We used the following strategy to assign each melting transition to a specific portion of the IRE: transitions in which the T_m was significantly affected by a mutation were assigned to a region that included that site and contained enough secondary structure to approximately match the ΔH determined by the curve-fitting analysis. If a mutation produced a T_m change in more than one transition, the transition that was most affected was matched with the region containing that mutation, and the other affected transitions were assigned to adjacent domains. Analysis of the melting curves of each of the mutants (with the exception of the Pavia 2 mutant) yielded two transitions for which the T_m and ΔH remained essentially unchanged, one transition that showed changes in T_m and ΔH for mutations that occurred in both the upper stem and loop (Paris 1, London 1, London 2), and a fourth transition that predominantly showed changes when the mutations occurred in the vicinity of the bulged C (Paris 2, Pavia 1) (Fig. 5*a*). This pattern allowed us to confidently pair the transition at $T_m = 48.5$ °C (T1) with the region just below the bulged C and the transition at $T_m = 58.6$ °C (T2) with the upper stem and loop (Fig. 5*b*). Although the precise regions corresponding to the transitions at 60.7 °C (T3) and 67.9 °C (T4) are difficult to assign because of the shortage of mutational information from that part of the IRE, the dramatic change in the T4 portion of the melting curve of Pavia 2 (Fig. 4, *Pavia 2 panel*) suggests that T4 includes the helix (C18:G62 to U26:A54) in which the Pavia 2 mutations occur. The thermodynamic parameters derived from each RNA are listed in Table III. Because we were uncertain of the changes in secondary structure in the Pavia 2 mutant, we were unable to derive thermodynamic information from the Pavia 2 melting curve.

DISCUSSION

Among the numerous genetic disorders that have been identified and studied, HHCS has emerged as a novel disease that arises from mutations within the protein-binding site of an RNA regulatory element. The mutations associated with HHCS occur throughout the IRE of the L-ferritin transcript and are so far the only naturally occurring mutations known to disrupt IRP recognition in a living organism. The clinical severity of HHCS is remarkably varied; serum ferritin levels can range anywhere from 2- to 10-fold higher than normal, and lens opacities can be severe enough to require surgical intervention or mild enough to have no detectable effect on visual acuity.

The measurements of the *in vitro* affinities of IRP1 and IRP2 for IREs containing HHCS mutations revealed that these mutations had variable effects on IRP binding. Relative dissociation constants ranged from 1.5 (Pavia 2) to 2200.0 (Verona) for IRP1, for a nearly 1500-fold difference in effect, and from 1.7 (Pavia 2) to 220.0 (Verona) for IRP2, or a 130-fold difference. We also found that with every mutation, except Pavia 2, the affinity for IRP1 was more affected than for IRP2. Studies of nonconsensus IRP-binding sequences have shown that, in general, IRP2 has a greater tolerance for mutations within the hexanucleotide loop of the IRE (23, 24). Additionally, the IRE binding capacity of IRP2 is much less affected by mutagenesis of individual arginines within the putative IRE-binding site (23). The diminished sensitivity of IRP2 to IRE mutations is

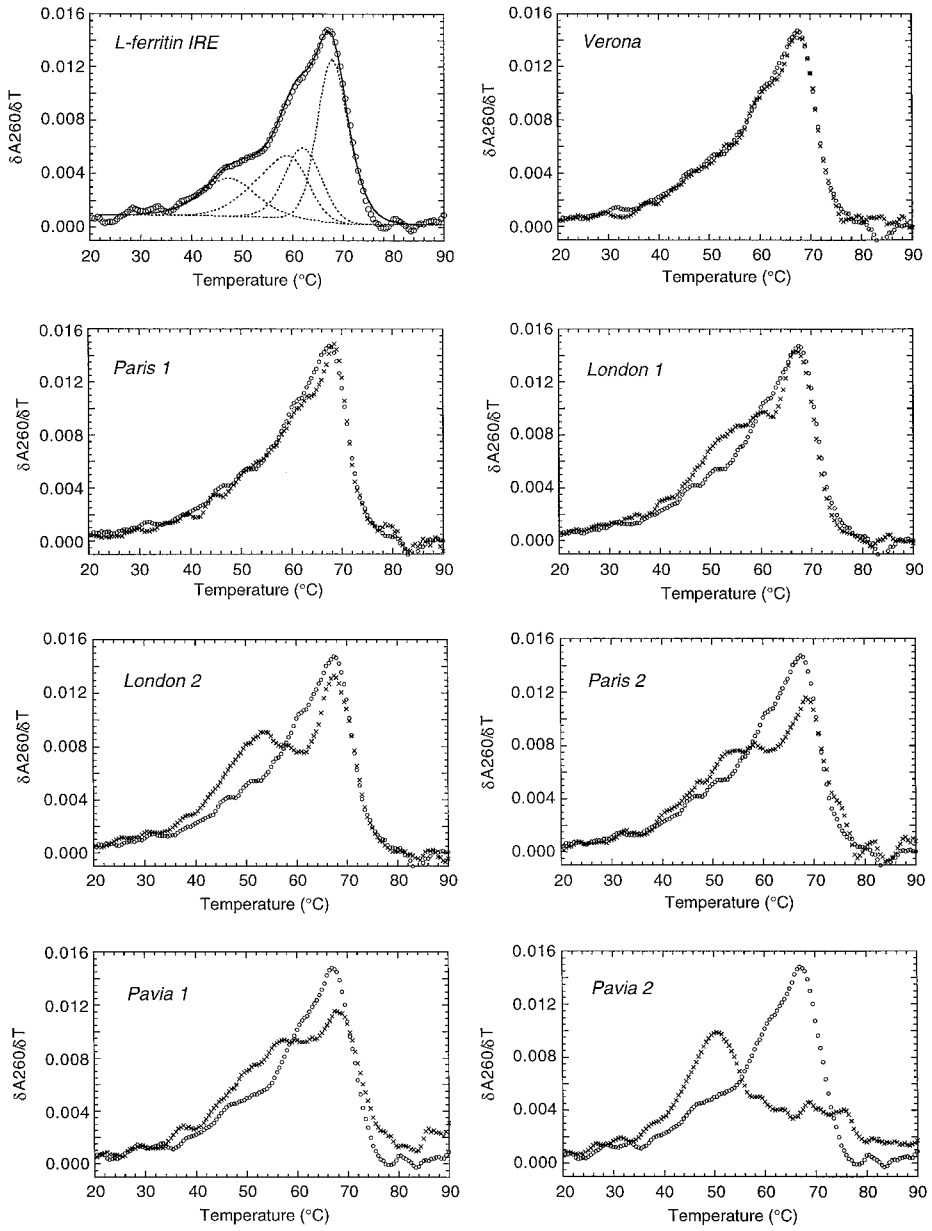

FIG. 4. **Absorbance melting curves of IREs containing HHCS mutations.** The absorbance at 260 nm was collected at 0.5 °C intervals as a 1.0 μM sample of each IRE was heated from 18 to 95 °C at a rate of 0.5 °C/min. The partial first derivative of the absorbance with respect to temperature ($\delta A_{260}/\delta T$) was calculated to yield the melting curves shown above. In each case, the $\delta A_{260}/\delta T$ of the wild-type L-ferritin IRE is shown in overlay (*open circles*) to highlight the differences in the melting curves of the mutants (*x*). The *dashed lines* in the L-ferritin IRE panel are representative of the four sequential transitions that were fitted to each data set (the *solid line* is the theoretical melting curve for these transitions), with the sole exception of the Pavia 2. The thermodynamic parameters derived from the melting curves are listed in Table IV.

further highlighted by the effects of the HHCS mutations, although the ranking of the HHCS mutations from lowest to highest affinity remains the same for both IRPs.

The reported concentration of serum ferritin for each HHCS mutation covers a wide range and may reflect the influence of non-HHCS factors, such as inflammation, cancer, and pathogenic infection, that are known to affect ferritin expression (33). We anticipated that this variability might mask correlations between binding affinity and serum ferritin levels; yet we discovered a significant correlation between serum ferritin levels and K_{Rel} for both IRPs and an even stronger correlation between the K_{Rel} and maximum serum ferritin. With such strong correlations for both IRPs, these experiments do not identify either protein as the predominant contributor to HHCS. The sharp transition from low (wild-type and Pavia 2) to relatively high (London 1) maximum serum ferritin with increasing K_{Rel} implies that the affinity of the IRPs for the IRE is highly optimized for the consensus sequence. Even the appearance of a measurable difference in serum ferritin for patients with the weakly impaired Pavia 2 mutation illustrates the extreme sensitivity of the IRE-IRP system to slight perturbations in affinity. With regard to cataract, there also appears to be a correlation between cases of HHCS requiring surgical intervention and mutations with the largest values of K_{Rel}. More subtle correlations between K_{Rel} and severity might easily be masked by other genetic or environmental factors thought to influence cataractogenesis, including differences in diet, exposure to UV light, or substance abuse (34).

Despite the correlation between serum ferritin levels and the effect of each HHCS mutation on the binding of IRPs, the mechanism by which L-ferritin reaches the serum is unclear. Ferritin appears in human serum even under normal conditions, and consists predominantly, if not exclusively, of L-ferritin (35). There have also been reports of glycosylated forms of ferritin in the serum (36, 37), implicating a secretory origin for a portion of serum ferritin. Although neither L- or H-ferritin has a classical signal peptide for targeting the nascent protein to the endoplasmic reticulum, L-ferritin has a short stretch of hydrophobic residues near the N terminus that might permit translocation to the ER. Several studies have detected elevated

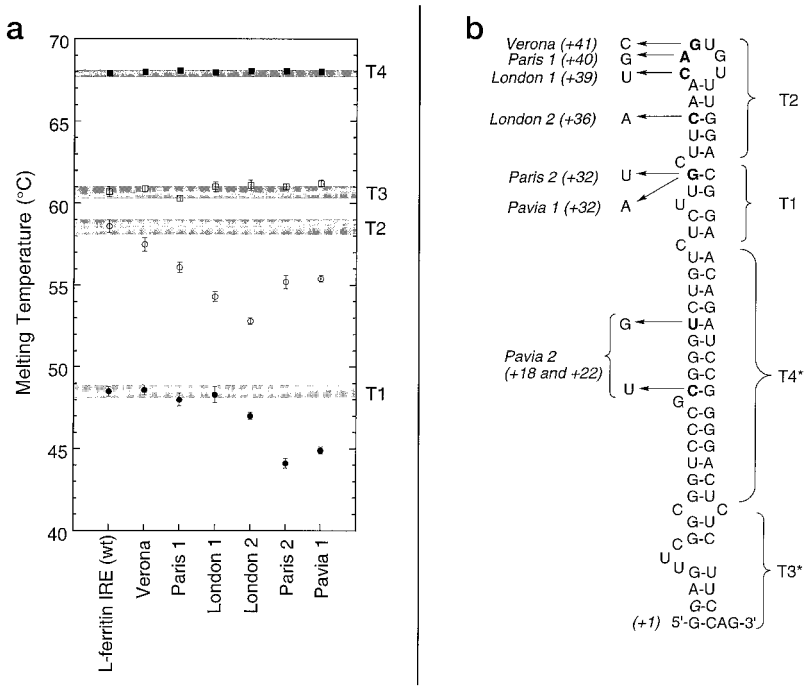

FIG. 5. **Assignment of the melting curve transitions to specific regions of IRE secondary structure.** *a*, plot of the T_m values from the four sequential transitions of the L-ferritin IRE and IREs containing the HHCS mutations. Whenever a value ± 1 S.D. fell outside of the range of the wild-type L-ferritin IRE (*leftmost data set*), the value of the T_m was deemed to be significantly different from the wild-type sequence. *b*, correlations between changes in T_m and site of mutation and comparisons of theoretical and actual ΔH were used to assign the four thermodynamic transitions to specific regions of the IRE. Although we believe that T3 and T4 encompass the entire region below T1, the boundaries of T3 and T4 cannot be confidently determined from the data.

intracellular levels of L-ferritin in cell lines and cultured tissues from HHCS patients (7, 38), suggesting that both the intracellular and serum forms of L-ferritin are expressed from the same misregulated gene. It is possible that when L-ferritin is translated in serum monocytes it is partitioned into both the ER and the cytosol and that the ER fraction is secreted into the serum. This partitioning could also serve as an additional point of regulation and might explain some of the variation in levels of serum ferritin in HHCS patients. The mechanism leading to cataract formation is also unknown, but a recent study has suggested that it might involve perturbations of the redox status of the lens (38).

We also wondered what these mutations might reveal about the structure of the IRE and its interactions with the IRPs. Although little is known about the three-dimensional structure of IRP1 or IRP2 (39), there has been some success determining the structure of the consensus IRE. Unfortunately, it has been difficult to ascertain which aspects of the secondary and tertiary structure of the IRE are important for recognition by the IRPs, nor have the sites of any intermolecular contacts been firmly identified. In studies of the consensus IRE (22), the effects of single point mutations on IRP affinity have been measured in an effort to identify sites of contact. Although measurable effects may indicate the loss of base-specific contacts, they might also reflect changes in the stability or secondary structure of the IRE. We recognized that some of the HHCS mutations might also act by disrupting important secondary structural elements of the IRE, including the A-form helix of the lower stem (Paris 2, Pavia 1, and Pavia 2), the extra-helical conformation of the bulged cytosine (Paris 2 and Pavia 1), the A-form helical conformation of the upper stem (London 2), the intraloop base pair (London 1), and the base-stacking interactions within the loop (Paris 1) (27–29). To elucidate any effects of the HHCS mutations on the structural conformation of the IRE, we measured the melting curves of the mutant IREs and calculated differences in their thermodynamic stabilities as reflected by $\Delta\Delta G_{25}$(IRE). The comparison of these changes with $\Delta\Delta G_{25}$(complex) allowed us to begin to understand the effects of many of the HHCS mutations.

The Verona mutation caused the largest loss in affinity for IRP1 and IRP2; yet its melting curve and the thermodynamic stability were nearly identical to the wild-type sequence, with a $\Delta\Delta G_{25}$(IRE) of only 0.5 kcal/mol. NMR analyses of the IRE have shown that the guanosine normally found at this position is solvent-exposed and structurally dynamic (25, 27), and cleavage assays have identified this position as being particularly sensitive to chemical reagents (40, 41). These observations, together with the thermodynamics of the Verona mutant, suggest that the consensus guanosine in that position is involved in an interaction with the IRPs worth between 2.8 and 4.1 kcal/mol.

The Paris 1 mutation also had relatively little effect on the energetics of the IRE loop, producing a $\Delta\Delta G_{25}$(IRE) that is insufficient to account for all of $\Delta\Delta G_{25}$(complex) for either IRP. In the consensus IRE, the adenine normally found at this position has been shown to be stacked on top of the intra-loop C1-G5 base pair (25). Replacement of the consensus adenine with guanosine might alter the orientation of this stacking interaction, but such a change is unlikely to produce a large $\Delta\Delta G_{25}$(complex). Although SELEX experiments have confirmed the preference for adenosine at this site, one study found cytidine in several IRP-binding clones and guanosine in a single IRP2-specific sequence containing multiple nonconsensus nucleotides (23), whereas the other identified cytidine- and uridine-containing sequences (24). The tolerance of substitutions other than guanosine at this site suggests that this nucleobase may be involved in a stacking interaction with the IRP and that the large size of guanosine may disrupt this association under most conditions. Such an interaction could account for the observed changes in affinity and leaves open the possibility that this base becomes unstacked in the IRE·IRP complex.

The London 1 mutation occurs in the position that has been shown by NMR to form a base pair with the fifth nucleotide in the hexaloop (25, 26). The mutation of C-39 to a U would eliminate Watson-Crick pairing with G-5 but would still permit the formation of a U-G base pair. We would expect this interaction to be weaker than the normal C-G base pair, an expectation that was confirmed by a drop in the T_m(T2) of 4.3 °C and a corresponding $\Delta\Delta G_{25}$(IRE) of 1.2 kcal/mol. This is nearly identical to the $\Delta\Delta G_{25}$(complex) for both IRP1 (1.3 kcal/mol) and IRP2 (1.0 kcal/mol). Thus, it is likely that most of the

TABLE III

Thermodynamic characteristics for IREs containing HHCS mutations

The melting curves ($\delta A_{260}/\delta T$) were fitted to four sequential transitions using the MeltFit package, from which was determined the parameters T_m and ΔH (see "Experimental Procedures" and Fig. 4). The averages ± 1 S.D. of T_m and ΔH are reported for at least four independent melting experiments and curve fits. Each helix/transition was assigned to a region of the IRE from the correlation of T_m with the known location of the mutation (see Fig. 5). ΔG_{25} for each transition was calculated from $\Delta G_{25} = \Delta H\ (1 - T/T_m)$. ΔS_{25} was calculated from $\Delta S_{25} = (\Delta H - \Delta G_{25})/T$ $\Delta\Delta G_{25}$(IRE) = ΔG_{25}(T1 + T2) (L-ferritin) − ΔG_{25}(T1 + T2) (mutant).

Mutation	Helix/transition	T_m	ΔH	ΔG_{25}	ΔS_{25}	ΔG_{25}(T1 + T2)	$\Delta\Delta G_{25}$(IRE)
		°C	kcal/mol		e.u.	kcal/mol	
L-ferritin IRE	T1	48.5 ± 0.3	45 ± 2	3.3	140	8.0	0.0
	T2	58.6 ± 0.4	46 ± 4	4.7	138		
	T3	60.7 ± 0.3	75 ± 2	8.0	220		
	T4	67.90 ± 0.06	108 ± 2	13.6	317		
Verona	T1	48.6 ± 0.3	44 ± 2	3.2	137	7.5	0.5
	T2	57.5 ± 0.4	44 ± 2	4.3	133		
	T3	60.9 ± 0.2	79 ± 3	8.5	236		
	T4	67.97 ± 0.08	107 ± 2	13.5	314		
Paris 1	T1	48.0 ± 0.4	43 ± 1	3.1	134	7.4	0.6
	T2	56.1 ± 0.3	46 ± 3	4.3	140		
	T3	60.3 ± 0.2	80 ± 2	8.5	240		
	T4	68.04 ± 0.04	111 ± 4	14.0	325		
London 1	T1	48.3 ± 0.5	43 ± 2	3.1	134	6.8	1.2
	T2	54.3 ± 0.3	42 ± 4	3.7	128		
	T3	61.0 ± 0.3	76 ± 6	8.2	227		
	T4	67.94 ± 0.07	110 ± 2	13.8	323		
London 2	T1	47.0 ± 0.2	43 ± 1	3.0	134	7.8	0.2
	T2	52.8 ± 0.2	56 ± 3	4.8	172		
	T3	61.1 ± 0.3	78 ± 4	8.4	233		
	T4	68.01 ± 0.06	107 ± 2	13.5	314		
Paris 2	T1	44.1 ± 0.3	36 ± 1	2.2	113	6.9	1.1
	T2	55.2 ± 0.4	51 ± 2	4.7	155		
	T3	61.0 ± 0.2	81 ± 4	8.7	242		
	T4	68.01 ± 0.05	106 ± 3	13.4	311		
Pavia 1	T1	44.9 ± 0.2	35 ± 1	2.2	110	6.3	1.7
	T2	55.4 ± 0.2	44 ± 2	4.1	134		
	T3	61.2 ± 0.2	76 ± 4	8.2	227		
	T4	67.98 ± 0.03	108 ± 2	13.6	317		

destabilization of the London 1 IRE·IRP complex arises from the weakened base pairing interaction, which leads in turn to a less favorable entropy change upon binding of the IRP.

The London 2 mutation might be expected to lead to a loss of base pairing, with the subsequent destabilization of the T2 domain. It does cause a drop in T_m(T2), plus a small loss in T_m(T1), but causes a $\Delta\Delta G_{25}$(IRE) of only 0.2 kcal/mol resulting from a gain in enthalpy of 10 kcal/mol and an entropic penalty of 34 e.u. In this mutant, the upper portion of the IRE could adopt an alternative conformation in which U-34 through C-39 pair with G-43 through G-48. This alternative secondary structure would be predicted to have an increase of 15 kcal/mol in ΔH and 0.2 kcal/mol in ΔG in comparison to the consensus fold and would place C-33 in a mismatch with A-49. Although the predicted energies of such a fold are in close agreement to what we measured, it seems likely that such a dramatic rearrangement would more severely impair the binding of IRPs. An alternative possibility is that this mutation forms a non-Watson-Crick A:G base pair that allows the preservation of the upper stem. The mismatch would probably distort the normal A-form helix geometry, and might force one of the A:G bases into a *syn*-glycosidic conformation (42, 43). A recent report has identified a nonfunctional IRE in the mouse glycolate oxidase transcript that has an A:A mismatch at the same site (44). In that example, the putative IRE retains its affinity for IRPs at room temperature but loses virtually all affinity at 37 °C. The London 2 mutant, however, binds poorly even at 25 °C, despite the minimal effects on $\Delta\Delta G_{25}$(IRE). From the sequences of naturally occurring IREs, we know that there is no discernible base pair preference in the upper stem, but there may be IRP contacts involving the RNA backbone. The changes in helix geometry arising from an A:G mismatch may be sufficient to disrupt backbone contacts and account for the loss in binding affinity.

Both of the Paris 2 and Pavia 1 mutations give rise to moderate values of $\Delta\Delta G_{25}$(IRE) (1.1 and 1.7 kcal/mol, respectively). Yet, the Paris 2 mutation causes a much larger $\Delta\Delta G_{25}$(complex). It has been shown that the unpaired cytosine normally adopts an extrahelical conformation and is structurally dynamic (25) and that the tendency of an unpaired nucleotide to stack within the helix is dependent upon the sequence of adjacent base pairs (45). Therefore, we might expect these mutations to alter the stacking preferences of the otherwise bulged C-33. We found that the $\Delta\Delta H$(T1) of 10 kcal/mol for the Paris 2 mutation is accompanied by an increase in ΔH(T2) of 7 kcal/mol, suggesting that a stacking interaction has shifted

from the T2 domain to the T1 domain. This may indicate that the normally bulged C-33 has adopted an intrahelical, stacked conformation. Such a conformational change would mask the identity of the highly conserved C-33 and may prevent the formation of intermolecular contacts. The energy required to extrude C-33 from the helix may account for a portion of $\Delta\Delta G_{25}$(complex). Although the Pavia 1 mutant also has a similar decrease in ΔH(T1), the absence of a compensatory change in ΔH(T2) makes it less likely that the extrahelical conformation of C-33 is being altered.

Perhaps the most dramatic result from the thermal denaturation studies is the change in the melting curve profile of the Pavia 2 mutant. Despite the retention of near wild-type affinity for both IRP1 and IRP2, the melting curve suggests a complete change in the thermodynamic behavior of this RNA. Analysis of the predicted lowest energy secondary structures of the Pavia 2 IRE shows that the energy differences between the fold assumed in this study and alternate folds are much smaller than with the wild-type sequence (data not shown). Because the two mutations in this sequence are outside of the recognized IRP binding footprint (39), it is also unlikely that direct contacts are being lost. One possibility is that changes in the stability of the lower region of the IRE result in an altered fold of the RNA that retains the appropriate secondary structure in the IRP-binding regions of the IRE sequence.

The Pavia 2 mutation illuminates what might be the primary function of the lower stem of the IRE. The thermodynamic behavior of Pavia 2 indicates that the IRP-binding domain, comprised of T1 and T2 in this study, is intact and sufficiently stable to retain the secondary structure required for functional activity. The lower stem serves as an additional regulatory element in that its length and G-C content fine-tune the stability of the IRE, modulating the sensitivity of a transcript to IRP-mediated translational control. This model is supported by studies showing that the translation of ferritin is more sensitive to changes in cellular iron status than mitochondrial aconitase, which has a shorter, A-U rich lower stem in its IRE (46).

The recent discovery and characterization of hereditary hyperferritinemia-cataract syndrome has provided a unique opportunity to understand the effects of IRE mutations on the behavior of the IRP regulatory process in a living organism. The diversity of HHCS-causing mutations is remarkable, and we speculate that many more HHCS mutations will eventually be found. As the medical community continues to identify new mutations, it will be important to note those nucleotide positions that never seem to be affected in HHCS. We believe that there may be naturally occurring polymorphisms within the L-ferritin IRE that do not affect IRP binding, or perhaps some that enhance binding, but the absence of a known phenotype will make it difficult to identify such variations. For each new mutation that does affect IRP binding, however, we can perform similar thermodynamic analyses and further refine our understanding of the exquisite recognition of IREs by IRP1 and IRP2.

REFERENCES

1. Girelli, D., Oliviero, O., De Franceschi, L., Corrocher, R., Bergamaschi, G., and Cazzola, M. (1995) *Br. J. Haematol.* **90,** 931–934
2. Bonneau, D., Winter-Fuseau, I., Loiseau, M.-N., Amati, P., Berthier, M., Oriot, D., and Beaumont, C. (1995) *J. Med. Genet.* **32,** 778–779
3. Beaumont, C., Leneuve, P., Devaux, I., Scoazec, J.-Y., Berthier, M., Loiseau, M.-N., Grandchamp, B., and Bonneau, D. (1995) *Nat. Genet.* **11,** 444–446
4. Girelli, D., Corrocher, R., Bisceglia, L., Olivieri, O., De Franceschi, L., Zelante, L., and Gasparini, P. (1995) *Blood* **86,** 4050
5. Aguilar-Martinez, P., Biron, C., Masmejean, C., Jeanjean, P., and Schved, J.-F. (1996) *Blood* **88,** 1895
6. Merkt, J. D. (1997) *Dtsch. Med. Wochenschr.* **122,** 504–506
7. Cazzola, M., Bergamaschi, G., Tonon, L., Arbustini, E., Grasso, M., Vercesi, E., Barosi, G., Bianchi, P. E., Cairo, G., and Arosio, P. (1997) *Blood* **90,** 814–821
8. Girelli, D., Corrocher, R., Bisceglia, L., Olivieri, O., Zelante, L., Panozzo, G., and Gasparini, P. (1997) *Blood* **90,** 2084–2088
9. Arnold, J. D., Mumford, A. D., Lindsay, J. O., Hegde, U., Hagan, M., Hawkins, J. R. (1997) *Gut* **41,** 408–410
10. Martin, M. E., Fargion, S., Brissot, P., Pellat, B., and Beaumont, C. (1998) *Blood* **91,** 319–323
11. Mumford, A. D., Vulliamy, T., Lindsay, J., and Watson, A. (1998) *Blood* **91,** 367–368
12. Cicilano, M., Zeccgina, G., Roetto, A., Bosio, S., Infelise, V., Stefani, S., Mazza, U., and Camaschella, A. (1999) *Haematologica* **84,** 489–492
13. Harrison, P. M., and Arosio, P. (1996) *Biochim. Biophys. Acta* **1275,** 161–203
14. Klausner, R. D., Rouault, T. A., and Harford, J. B. (1993) *Cell* **72,** 19–28
15. Hentze, M. W., and Kuhn, L. C. (1996) *Proc. Natl. Acad. Sci. U. S. A.* **93,** 8175–8182
16. Gray, N. K., and Hentze, M. W. (1994) *EMBO J.* **13,** 3882–3891
17. Muckenthaler, M., Gray, N. K., and Hentze, M. W. (1998) *Mol. Cell* **2,** 383–388
18. Rouault, T. A., and Klausner, R. D. (1996) *J. Bioinorg. Chem.* **1,** 494–499
19. Hentze, M. W., and Kühn, L. C. (1996) *Proc. Natl. Acad. Sci. U. S. A.* **93,** 8175–8182
20. Iwai, K., Klausner, R. D., and Rouault, T. A. (1995) *EMBO J.* **14,** 5350–5357
21. Guo, B., Phillips, J. D., Yu, Y., and Leibold, E. A. (1995) *J. Biol. Chem.* **270,** 21645–21651
22. Jaffrey, S. R., Haile, D. J., Klausner, R. D., and Harford, J. B. (1993) *Nucleic Acids Res.* **21,** 4627–4631
23. Butt, J., Kim, H.-Y., Basilion, J. P., Cohen, S., Iwai, K., Philpott, C. C., Altschul, S., Klausner, R. D., Rouault, T. A. (1996) *Proc. Natl. Acad. Sci. U. S. A.* **93,** 4345–4349
24. Henderson, B. R., Menotti, E., and Kühn, L. C. (1996) *J. Biol. Chem.* **271,** 4900–4908
25. Addess, K. J., Basilion, J. P., Klausner, R. D., Rouault, T. A., and Pardi, A. (1997) *J. Mol. Biol.* **274,** 72–83
26. Laing, L. G., and Hall, K. B. (1996) *Biochemistry* **35,** 13586–13596
27. Hall, K. B., and Tang, C. (1998) *Biochemistry* **37,** 9323–9332
28. Milligan, J. F., Groebe, D. R., Witherell, G. W., and Uhlenbeck, O. C. (1987) *Nucleic Acids Res.* **15,** 8783–8798
29. Samaniego, F., Chin, J., Iwai, K., Rouault, T. A., Klausner, R. D. (1994) *J. Biol. Chem.* **269,** 30904–30910
30. Drake, S. K., Lee, K. L., and Falke, J. J. (1996) *Biochemistry* **35,** 6697–6705
31. Draper, D. E., and Gluick, T. C. (1995) *Methods Enzymol.* **259,** 281–305
32. Serra, M. J., and Turner, D. H. (1995) *Methods Enzymol.* **259,** 242–261
33. Lee, M. H., and Means, R. T. (1995) *Am. J. Med.* **98,** 566–571
34. Trudo, E. W., and Stark, W. J. (1998) *Postgrad. Med.* **103,** 114–116
35. Santambrogio, P., Cozzi, A., Levi, S., and Arosio, P. (1987) *Br. J. Haematol.* **65,** 235–237
36. Cragg, S. J., Wagstaff, M., and Worwood, M. (1981) *Biochem. J.* **199,** 565–571
37. Santambrogio, P., Cozzi, A., Levi, S., and Arosio, P. (1987) *Br. J. Haematol.* **65,** 235–237
38. Levi, S., Girelli, D., Perrone, F., Pasti, M., Beaumont, C., Corrocher, R., Albertini, A., and Arosio, P. (1998) *Blood* **91,** 4180–4187
39. Basilion, J. P., Rouault, T. A., Massinople, C. M., Klausner, R. D., and Burgess, W. H. (1994) *Proc. Natl. Acad. Sci. U. S. A.* **91,** 574–578
40. Thorp, H. H., McKensie, R. A, Lin, P.-N., Walden, W. E., and Theil, E. C. (1996) *Inorg. Chem.* **35,** 2773–2779
41. Ciftan, S. A., Theil, E. C., and Thorp, H. H. (1998) *Chem. Biol.* **5,** 679–687
42. Morse, S. E., and Draper, D. E. (1995) *Nucleic Acids Res.* **23,** 302–306
43. Gautheret, D., Konings, D., and Gutell, R. R. (1994) *J. Mol. Biol.* **242,** 1–8
44. Kohler, S. A., Menotti, E., and Kühn, L. C. (1999) *J. Biol. Chem.* **274,** 2401–2407
45. Bhattacharyya, A., Murchie, A. I., and Lilley, D. M. (1990) *Nature* **343,** 484–487
46. Kim, H.-Y., LaVaute, T., Iwai, K., Klausner, R. D., and Rouault, T. A. (1996) *J. Biol. Chem.* **271,** 24226–24230